ELSEVIER

Journal of Fluids and Structures 20 (2005) 961–974

JOURNAL OF FLUIDS AND STRUCTURES

www.elsevier.com/locate/jfs

On the flow over a rotationally oscillating flat plate: A numerical study

J.M. Chen*, Y.-C. Fang

Department of Mechanical Engineering, National Chung Hsing University, Taichung 402, Taiwan

Received 20 April 2004; accepted 18 May 2005

Abstract

The characteristics of the flow in the wake of a plate that is normal to the free stream in its neutral position undergoing rotational oscillation has been investigated. The governing equations based on stream-function/vorticity formulation are solved numerically to determine the two-dimensional flow field structure. The numerical simulations are performed in a rotating reference frame attached to the plate. The simulations focus on the lock-on phenomenon of vortex shedding for frequency ratios of forcing Strouhal number to natural shedding Strouhal number $St_e/St_n = 0.96$–1.04 at a Reynolds number $Re = 100$. The time histories of drag coefficient as well as surface vorticity of the plate show amplitude modulation when the vortex shedding is not-locked-on to the plate oscillation at smaller forcing amplitude. The modulation disappears once lock-on occurs where the vortex shedding is synchronized with the plate oscillation at larger amplitude. The limits of lock-on regime bounded by the forcing frequency and amplitude are found in good agreement with the experiments conducted at higher Reynolds numbers ($Re = 3600-9800$). For the approach to lock-on from a lower frequency ($St_e/St_n = 0.96$) and an upper frequency ($St_e/St_n = 1.04$), the numerical simulations demonstrate significant differences in lock-on behavior, including the structure of vortices, fluctuation amplitudes of drag coefficient and surface vorticity, and route leading to lock-on.

Keywords: Vortex shedding; Lock-on; Oscillating plate

1. Introduction

It is well known that periodic shedding of vortices from a bluff body may result in fluctuating forces on the body. When the incident mean flow or the body is forced to oscillate with sufficiently large amplitude at a frequency that is close to the natural shedding frequency, the vortex shedding can be synchronized with the forced oscillation. The synchronization of vortex shedding is commonly called the lock-on phenomenon (Blevins, 1990). The lock-on of vortex shedding to an external forcing provides potential means for active control of the wake flow behind a bluff body.

The studies on the oscillating bluff body flow can be divided into two categories depending on the motion of the body. The first category is for the body undergoing either an in-line or transverse oscillation with respect to the free stream [e.g. Griffin and Ramberg (1976), Ongoren and Rockwell (1988a, b)]. The other is the body oscillating rotationally about its axis across the mean flow. In contrast to numerous studies carried out for the first category, the

*Corresponding author. Tel.: +886 4 284 0433; fax: +886 4 2877170.
E-mail address: jerryc@dragon.nchu.edu.tw (J.M. Chen).

0889-9746/$ - see front matter © 2005 Elsevier Ltd. All rights reserved.
doi:10.1016/j.jfluidstructs.2005.05.006

number of studies on the second category appears relatively small but has rapidly increased recently. Nevertheless, the experimental and numerical studies on the second category mostly deal with the flow due to a rotationally oscillating circular cylinder (Tokumaru and Dimotakis, 1991; Filler et al., 1991, Baek and Sung, 2000; Mahfouz and Badr, 2000; Cheng et al., 2001; Choi et al., 2002). Comparatively, fairly few studies have reported on the flow past a rotationally oscillating flat plate. Unlike the case of the circular cylinder, the flow over a flat plate is characterized by fixed separation points at the edge of the plate. Moreover, in numerical simulations one should deal with a moving boundary condition on the rotating plate surface, rather than a fixed condition usually imposed on the rotating circular cylinder surface. Even for a stationary normal flat plate, the wake behind it demonstrates interesting complex dynamics (Najjar and Balachandar, 1998). Chua et al. (1990) have made numerical and experimental investigations of the separated flow over a laterally oscillating plate and reported transient variations in the flow field and the resultant aerodynamic characteristics. But, they did not show the vortex shedding that is locked-on with the forcing. Among the few reports on a rotationally oscillating flat plate, only Chen and Fang (1998) and Fang and Chen (2000) observed the lock-on of vortex shedding in wind tunnel experiments. However, due to limitations in the experiments, the detailed flow field of vortex lock-on and the effects of rotational oscillations of a flat plate remain unclear.

The present numerical study aims to investigate the characteristics of vortex lock-on for a rotationally oscillating flat plate that is normal to the free stream in its neutral position. The onset of vortex lock-on depends on the combination of the forcing frequency and amplitude of the oscillating plate. This study focuses on the flow behavior that may vary with the forcing Strouhal number St_e in a range of $0.96 \leqslant \mathrm{St}_e/\mathrm{St}_n \leqslant 1.04$, slightly above or below the natural shedding Strouhal number St_n behind the stationary normal plate. Within this forcing frequency range, the influence of forcing amplitude on the lock-on behavior is examined as well. The governing equations based on stream-function/vorticity formulation are solved numerically by a finite difference scheme to determine the two-dimensional flow field structure at a Reynolds number $\mathrm{Re} = 100$. The numerical simulations are performed in a rotating reference frame attached to the plate, which yields a simpler boundary condition on the surface of the rotationally oscillating plate. The numerical results are compared with the experiments of Chen and Fang (1998).

2. Numerical method

Fig. 1 illustrates the schematic of the physical model presented in an inertial coordinate system. A vertical zero-thickness plate of width H is placed in a uniform cross-stream with a free-stream velocity U. The plate is undergoing a sinusoidal rotational oscillation about its axis of the form

$$\theta = A_0 \sin(2\pi f_e t), \tag{1}$$

where θ is the angular displacement, t is the time, and A_0 and f_e are the angular displacement amplitude and frequency, respectively.

The present numerical study considers the two-dimensional flow of a viscous incompressible fluid. In order to simplify the boundary condition on the plate surface, the numerical simulations are based on the coordinates that are attached to the plate and rotating with its oscillating motion and the origin coincides with the rotation axis. The governing equations are expressed in terms of dimensionless vorticity ω_I and stream function φ_I in the inertial frame as follows:

$$\frac{\partial \omega_I}{\partial t} + u\frac{\partial \omega_I}{\partial x} + v\frac{\partial \omega_I}{\partial y} = \frac{1}{\mathrm{Re}}\nabla^2 \omega_I, \tag{2}$$

$$\frac{\partial^2 \varphi_I}{\partial x^2} + \frac{\partial^2 \varphi_I}{\partial y^2} = -\omega_I, \tag{3}$$

where the subscript I denotes the quantity measured in the inertial frame, the velocities u and v and the coordinates x and y are in the rotating frame, and $\mathrm{Re} = UH/v$ is the Reynolds number with v as the kinematic viscosity. The vorticity and stream function in the inertial frame are related to those in the rotating frames (ω and φ), respectively, by

$$\omega_I = \omega + 2\Omega, \tag{4}$$

$$\varphi_I = \varphi - \frac{\Omega r^2}{2}, \tag{5}$$

where Ω is the angular velocity of the plate and r denotes the radial position from the origin. All variables including t are herein nondimensionalized by the plate width H and the free-stream velocity U.

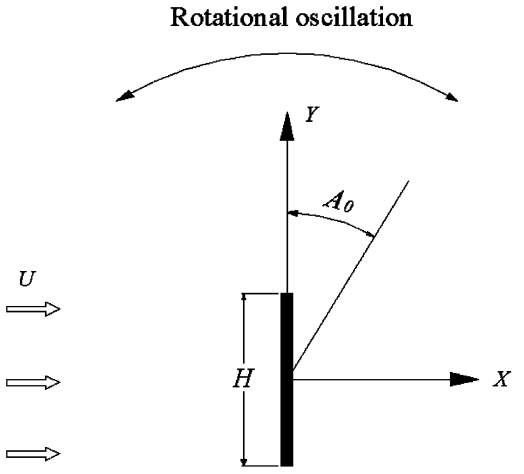

Fig. 1. Schematic of flow configuration in physical plane.

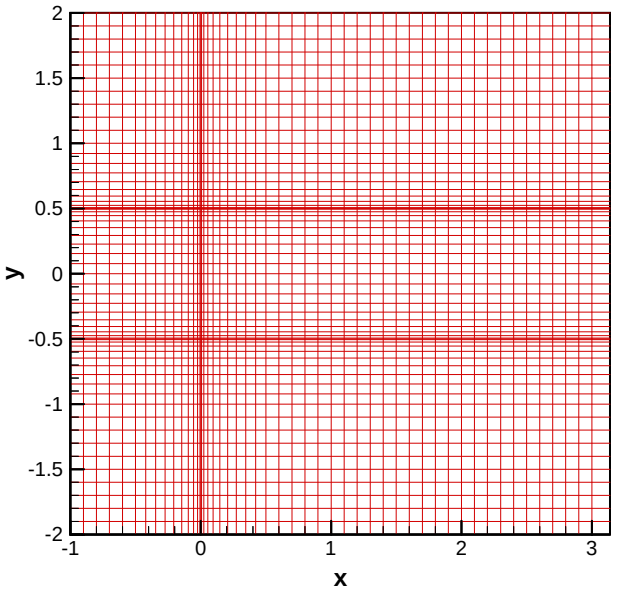

Fig. 2. Computational mesh.

The numerical simulations are carried out in the rotating coordinates with an appropriate computational grid for discretizing Eqs. (2) and (3). Fig. 2 shows part of the computational grid distribution in the $x-y$ coordinates, in which the plate is located at $x = 0$ and $-0.5 \leqslant y \leqslant 0.5$. The grid is nonuniformly distributed, with much more grid points in the vicinity of the plate to take account of rapid variations in this region. The nonuniform grid distribution can be mapped onto a computational domain (ξ, η) that contains a uniform grid distribution for implementation of the numerical programs using the finite difference method. The governing stream-function/vorticity equations in the computational domain are given as

$$\omega_{It} + uJy_{\eta}\omega_{I\xi} + vJx_{\xi}\omega_{I\eta} = \frac{1}{\mathrm{Re}}(a\omega_{I\xi\xi} + c\omega_{I\eta\eta} + d\omega_{I\eta} + e\omega_{I\xi}), \tag{6}$$

$$J^2(a\varphi_{I\xi\xi} + c\varphi_{I\eta\eta} + d\varphi_{I\eta} + e\varphi_{I\xi}) = -\omega_I, \tag{7}$$

where

$$a = y_\eta^2, c = x_\xi^2, d = -Jx_\xi\beta, e = -Jy_\eta\alpha, \alpha = ax_{\xi\xi} + cx_{\eta\eta},$$
$$\beta = ay_{\xi\xi} + cy_{\eta\eta}, J = x_\xi y_\eta.$$

Eqs. (6) and (7) in the coordinates (ξ, η, t) are solved with using a second-order central difference scheme in space and first-order backward Euler scheme in time. Here, we use the first-order implicit scheme rather than a higher-order explicit Runge–Kutta or implicit Crank–Nicolson method, for considerations of numerical stability and implementation of the simulations in the already complex rotating frame. When computing ω_I and φ_I of Eqs. (6) and (7), we employ the ADI (alternative-direction-implicit) technique that successively performs the ξ-sweep and η-sweep for the vorticity and then the ξ-sweep and η-sweep for the stream function. The convergence condition for time advancement is that root-mean-square (r.m.s.) of the residuals of Eqs. (2) and (3) for ω_I and φ_I, respectively, satisfies the following inequalities:

$$\mathrm{Rms}\left(\frac{\partial\omega_I}{\partial t} + u\frac{\partial\omega_I}{\partial x} + v\frac{\partial\omega_I}{\partial y} - \frac{1}{\mathrm{Re}}\nabla^2\omega_I\right) < 10^{-6}, \tag{8}$$

$$\mathrm{Rms}(\nabla^2\varphi_I + \omega_I) < 10^{-6}. \tag{9}$$

Moreover, the iterative successive over-relaxation (SOR) method is employed to solve the linear systems involved in the discretized stream function φ_{ij} and vorticity ω_{ij} as

$$\varphi_{ij}^{m+1} = \lambda\varphi_{ij}^{m+1} + (1-\lambda)\varphi_{ij}^{m}, \tag{10}$$

$$\omega_{ij}^{m+1} = \lambda\omega_{ij}^{m+1} + (1-\lambda)\omega_{ij}^{m}, \tag{11}$$

where λ is the acceleration parameter, and m denotes the iteration number. After several tests, an optimum acceleration parameter $\lambda = 1.93$ has been found for the convergence of the iterative processes.

To investigate the lock-on behavior of the vortices shedding from the rotationally oscillating plate, Eqs. (6) and (7) are solved with initial and boundary conditions that are compatible with the experiments of Chen and Fang (1998). The flow field obtained for the stationary plate is used as the initial condition for the flow simulations of oscillating plate. The boundary conditions to be satisfied are the no-slip and impermeability conditions on the plate surface and the inflow and outflow conditions at the upstream and downstream boundaries, respectively. The no-slip condition imposed on the plate surface is based on the rotating frame, for which the inertial quantities are expressed as

$$\varphi_I(x_w, y_w, t) = -\frac{\Omega(t)r^2}{2}, \tag{12}$$

$$\omega_I(x_w, y_w, t) = -\nabla^2\varphi(x_w, y_w, t) + 2\Omega(t), \tag{13}$$

where $\varphi(x_w, y_w, t) = 0$ on the plate surface. The uniform free-stream condition is used at the inflow boundary as well as on the upper and lower boundaries in the y-direction, where the stream function is considered constant and the vorticity is taken equal to zero along the boundaries. The floating condition is employed at the outflow boundary, where the derivatives of the stream function and vorticity in x-direction are taken equal to zero. The computational domain covers $-8 \leqslant x \leqslant 25$ and $-8 \leqslant y \leqslant 8$ with a resolution of 121×87 grid points, respectively, in the horizontal and vertical directions. The nonuniform grid as illustrated in Fig. 2 has grid sizes no larger than 0.1 in the neighborhood of the plate ($-1 \leqslant x \leqslant 4$ and $-2 \leqslant y \leqslant 2$), with the minimum size of 0.02 near the edges to capture the vortical structure being shed. A computational time step $\Delta t = 0.002$ is used to keep the maximum convective CFL number below 0.5. Convergence of the spatial and temporal resolutions is examined for the case of stationary normal plate at $\mathrm{Re} = 100$. It is found that doubling the grid resolutions in the x and y directions or halving the time step results in a change of less than 0.5% in the time-mean drag coefficient.

The distribution of pressure coefficient C_p along the plate surface may be obtained from the integration of the momentum equation that relates the pressure gradient to the vorticity flux across the plate surface into the fluid (Panton, 1984). For two-dimensional flow over an oscillating plate, the integration reads

$$C_p = -2\left[-\int_O^S \frac{1}{\mathrm{Re}}\frac{\partial\omega_I}{\partial n}\,\mathrm{d}s + \frac{\mathrm{d}\Omega}{\mathrm{d}t}\int_O^S (x\,\mathrm{d}y - y\,\mathrm{d}x) + \Omega^2(r_S^2 - r_O^2)\right], \tag{14}$$

where s is the position on the plate, n is the unit normal, $r_S = (x_S^2 + y_S^2)^{1/2}$ and $r_O = (x_C^2 + y_C^2)^{1/2}$, and the subscripts c and s represent the center and arbitrary positions on the plate, respectively. In the above equation, the second integral

term is identical to zero for the case of the present study since x and y are orthogonal to each other. Moreover, the derivative $\partial\omega_I/\partial n$ in the equation is computed using the second-order one-side formula. The drag coefficient can then be obtained by integration of C_p along the front and back surfaces of the plate:

$$C_D = -\oint C_p \frac{\mathrm{d}y}{\mathrm{d}s}\,\mathrm{d}s. \tag{15}$$

The numerical method was used to compute the flow over a stationary normal plate for verification prior to conducting numerical simulations of flow past a rotationally oscillating plate. For the stationary case, we have obtained $\mathrm{St}_n = 0.176$ and 0.174 for $\mathrm{Re} = 100$ and 126, respectively. These Strouhal numbers along with the corresponding flow structures and the transient growth in longitudinal formation length of the wake bubble behind the plate agree well with those obtained by previous investigators (Taneda and Honji, 1971; Tamaddon-Jahromi et al., 1994; Najjar and Vanka, 1995). The time-mean drag coefficient without blockage correction obtained is 2.91 for $\mathrm{Re} = 100$, which is in close agreement with value of 2.9 obtained by Najjar and Vanka (1995) in a simulation with high temporal and spatial resolutions at the same Reynolds number and blockage ratio (1/16).

3. Results and discussion

The computation is based on the rotating frame that is periodically oscillating about the rotation axis. When one tries to use the fluctuating velocity of the inertial frame for determination of vortex lock-on, interpolation must be carried out. The interpolation process could result in error to some extent as the plate oscillates with large displacement amplitude. In the present study, we use the time-varying values of the drag coefficient C_D as well as the vorticity W_o at the rotation axis on the back surface of the plate to determine the lock-on state.

Fig. 3 shows the time histories of C_D and W_o for non-lock-on and lock-on cases at a dimensionless oscillation frequency $\mathrm{St}_e/\mathrm{St}_n = 0.960$. The non-lock-on case that is computed at $A_0 = 15^\circ$ demonstrates amplitude modulation with a large modulation period. Notably, the maximum fluctuation in W_o corresponds to a rapid change of the fluctuation amplitude in C_D. The modulation phenomenon will be further examined later using the spectral analysis. As the oscillation amplitude increases to $A_0 = 20^\circ$, the shedding of vortices can be locked-on to the oscillating plate beginning at a dimensionless time around $t = 50$. Thereafter, the amplitude of C_D and W_o remain constant during the lock-on state. Synchronization of the vortex shedding with the oscillation of the plate can be examined by comparison of the phase evolution between the two motion traces. Figs. 4 and 5 illustrate the variations of the phase of C_D and W_o in reference to a fixed angular displacement position ($\theta = 0$) of the plate for the just-mentioned non-lock-on and lock-on cases, respectively. The trace of the neutral position of the plate is presented with a solid dot symbol in the figures. The time interval between the solid dots represents a half cycle of the plate oscillation in the C_D trace and a full cycle in the W_o trace. It can be seen that the shedding of vortices is synchronized with the motion of the plate for the lock-on case, and the neutral position corresponds to a maximum in C_D and nearly a minimum in W_o. This indicates that a vortex is alternatively shed from the upper and lower edges of the plate per half cycle and the vortices being shed are all equal in size. The synchronization does not occur for the non-lock-on case, for which both of the C_D and W_o traces show progressing phase lead against the plate oscillation due mainly to the slightly lower forcing frequency than the natural shedding frequency. Unlike the lock-on case, each of the vortices being shed at the alternating edges falls slightly short of a half cycle in the non-lock-on case, and the vortices vary in size. The variation of the vortex size takes a long period, as indicated in the modulated C_D and W_o traces.

As the vortices are shed from an oscillating plate, a periodic force is exerted on the plate. The streamwise component of the periodic force (i.e., the drag force) experienced by the plate will be at twice the frequency of the vortex shedding as well as the plate oscillation, while the frequency of the force component in the transverse direction (i.e., the lift force, which is relatively much smaller for the present case) are the same as the vortex-shedding frequency. The power spectra of C_D for the non-lock-on and lock-on cases are given in Fig. 6. In the non-lock-on spectrum, three frequency components dominate, namely the forcing frequency $\mathrm{St}_e = 0.169$, the vortex-shedding frequencies St_v, and the modulation frequencies St_m. The forcing component appears with a sharp, high peak in the spectrum at a dimensionless value of 0.338, that is twice St_e. The vortex-shedding frequencies St_v are slightly higher than the forcing frequency with a prominent frequency and shifting between 0.175 and 0.23, but mostly in a lower frequency band. The modulation in the non-lock-on case indicates a strong nonlinear interaction between the excited oscillation and the shedding of vortices. Therefore, the discrepancy between St_e and St_v results in rather low modulation frequencies St_m. This is evident in the spectrum showing St_m as a difference between St_e and St_v. In the present study, the modulation periods are found to be 190 in dimensionless time nearly identical for $\mathrm{St}_e/\mathrm{St}_n = 0.96$ at $A_0 = 10^\circ$ and 15° and 207 for

$St_e/St_n = 0.96$ at $A_0 = 10^\circ$, appearing to be more dependent on the forcing frequency than the forcing amplitude. Such a modulation phenomenon has also been observed in the simulations of flow past a circular cylinder subjected to rotational oscillations (Baek and Sung, 2000; Mahfouz and Badr, 2000; Choi et al., 2002) as well as one undergoing transverse oscillations (Anagnostopoulos, 2000). The modulation occurs typically when $St_e/St_n \approx 1$ at a forcing amplitude slightly lower than the lock-on threshold, which is referred to as the "receptivity region" by Karniadakis and Triantafyllou (1989). Choi et al. (2002) have recently discussed in detail the modulation phenomenon that occurs near $St_e/St_n \approx 1$ and at higher forcing frequencies. In the lock-on spectrum, only the forcing frequency and its higher harmonics appear prominent, indicating the synchronization of the vortex shedding with the plate oscillation. This observation of the spectra agrees with the experiment of Chen and Fang (1998).

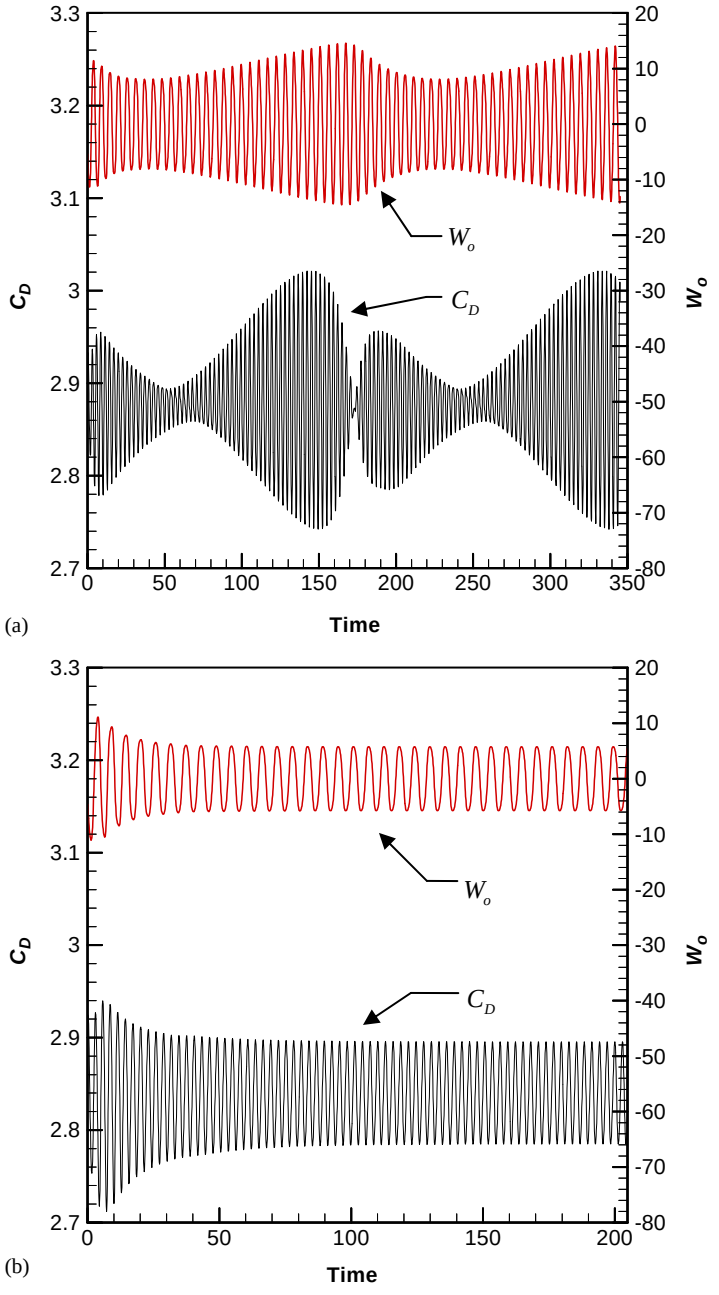

Fig. 3. Time histories of C_D and W_o at $St_e/St_n = 0.960$ for (a) non-lock-on ($A_0 = 15^\circ$) and (b) lock-on ($A_0 = 20^\circ$) cases.

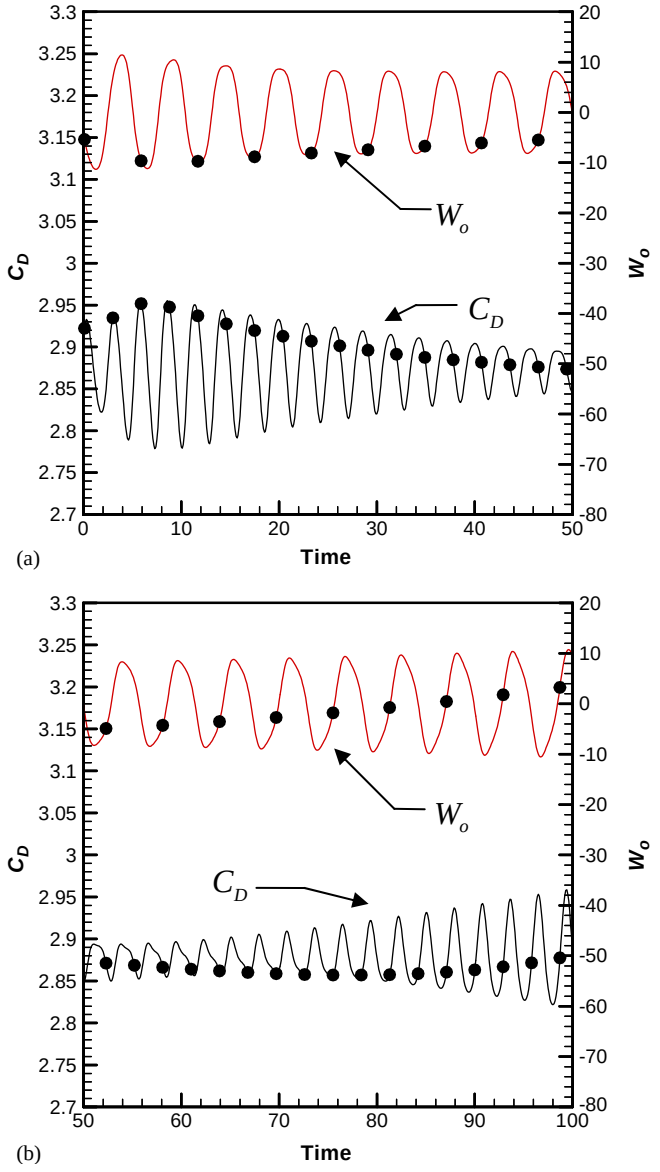

Fig. 4. Comparison of C_D and W_o time histories with plate motion (● denotes the neutral position, $\theta = 0$) at $St_e/St_n = 0.960$ for non-lock-on ($A_0 = 15^\circ$) case: (a) dimensionless time 0–50; (b) dimensionless time 50–100.

The state of vortex lock-on can be approached from either a lower forcing frequency ($St_e/St_n < 1$) or a upper forcing frequency ($St_e/St_n > 1$). Fig. 7 illustrates the lock-on time histories of C_D and W_o for an approach from an upper frequency of $St_e/St_n = 1.040$ at $A_0 = 20^\circ$. The comparison is made with the time histories of Fig. 5 showing an approach to lock-on from a lower frequency of $St_e/St_n = 0.960$ at the same forcing amplitude. During the early stages when the plate begins to oscillate from a stationary situation, the time histories show nearly the same pattern for the lower and upper frequency approaches, that is a growing amplitude up to $t = 10$. Thereafter, the fluctuation amplitudes of C_D and W_o remain constant for the case of the upper frequency ($St_e/St_n = 1.040$) approach, indicating a rapid reaching to the lock-on state. For the lower frequency approach, the amplitudes of C_D and W_o decrease gradually, until the lock-on state is reached at $t = 50$. The phenomenon that larger fluctuation of C_D and W_o for the upper frequency approach to the lock-on and smaller oscillation for the lower frequency approach is due largely to the strength as well as the position of the starting vortex that develops near the edge of the plate. Fig. 8 shows the streamline contours for

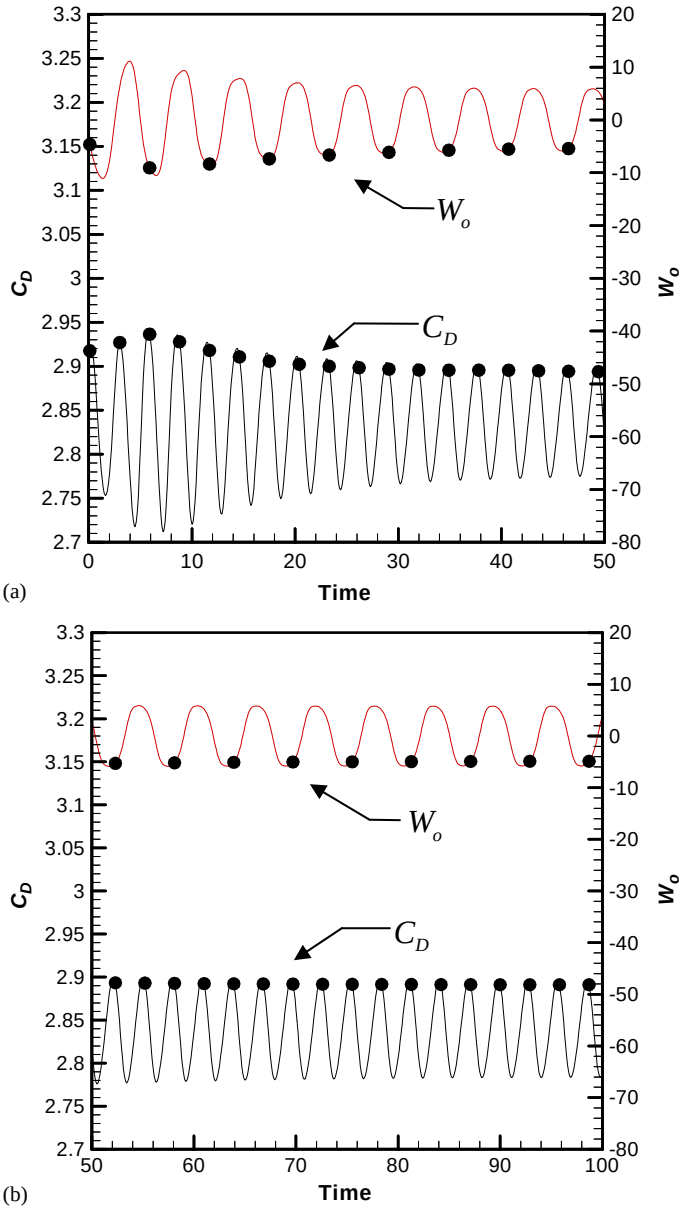

Fig. 5. Comparison of C_D and W_o time histories with plate motion (● denotes the neutral position $\theta = 0$) at $St_e/St_n = 0.960$ for lock-on ($A_0 = 20^\circ$) case: (a) dimensionless time 0–50; (b) dimensionless time 50–100.

$St_e/St_n = 1.040$, 1.0 and 0.960 at the same oscillation amplitude $A_0 = 20^\circ$. It can be seen that the center of the starting vortex appearing in the neighborhood of the lower edge of the plate at the same angular displacement position develops closer to the rear surface of plate as St_e/St_n increases from 0.960 to 1.040. The vortex developed closer to the plate surface with more compact structure (as will be seen in Fig. 9) results in larger amplitude in the time histories of the drag coefficient and surface vorticity at the rotation axis. The numerical results are consistent with the flow visualization of Chen and Fang (1998).

The approach to lock-on from upper or lower frequency forcing is expected to exhibit different vortex spacing in the wake (Anagnostopoulos, 2000). Fig. 9 shows the vorticity contours for $St_e/St_n = 1.040$ and 0.960 at the same oscillation amplitude $A_0 = 20^\circ$. It can be seen that the longitudinal vortex spacing, which is defined by the horizontal centers of consecutive vortices shed from the same edge of the plate, reduces from 4.6–4.8H to 4.0–4.2H as the forcing frequency

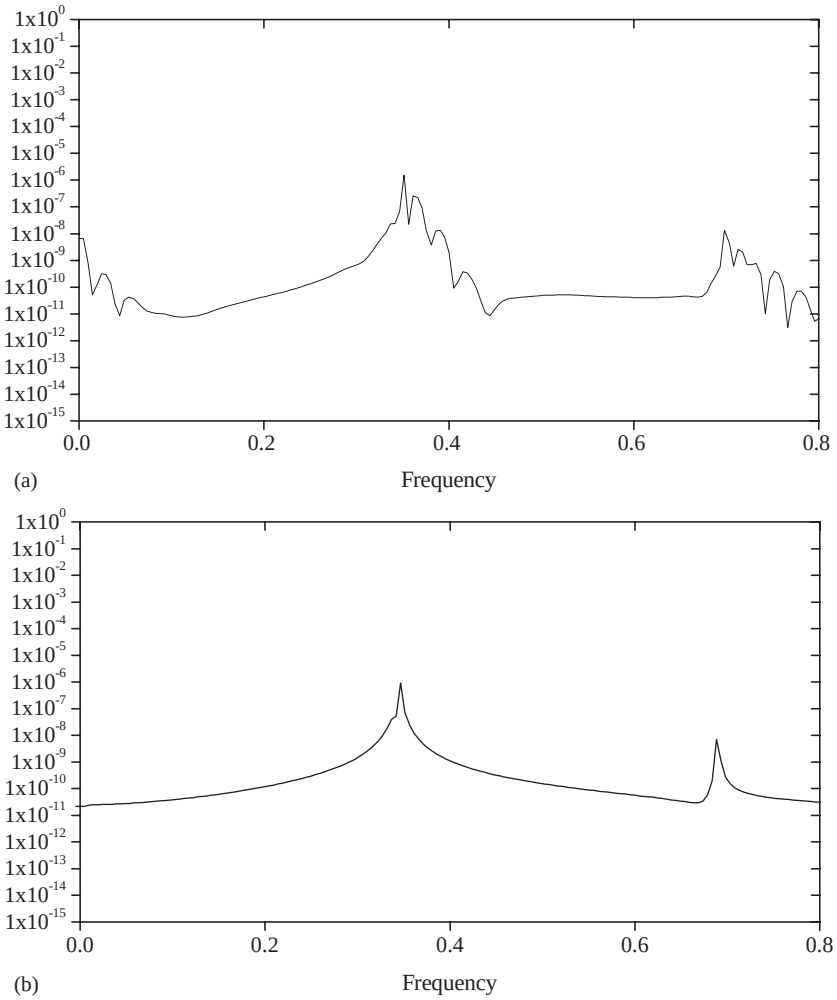

Fig. 6. Power spectra of drag coefficient at $St_e/St_n = 0.960$ for (a) non-lock-on ($A_0 = 15^\circ$) and (b) lock-on ($A_0 = 20^\circ$) cases.

increases from $St_e/St_n = 0.960$ to 1.040 in the wake region between $x = 3$ and 12. The vortex convection velocities in this region were estimated at 0.80 and $0.76U$ for $St_e/St_n = 0.960$ and 1.040, respectively. However, the lateral vortex spacing, which is defined by the vertical centers of consecutive vortices shed from the upper and lower edges of the plate, is about $2.4H$, essentially unaffected by the difference in forcing frequency.

It is also of interest to examine the effect of forcing amplitude on the lock-on vortical structure. Figs. 10 and 11 show the streamline and vorticity contours, respectively, computed at the same forcing frequency $St_e/St_n = 1.0$ for different oscillation amplitudes $A_0 = 10^\circ$ and 20°. Notice that vortex shedding at $St_e/St_n = 1.0$ can be locked-on to an arbitrarily small forcing amplitude in numerical simulation. As the forcing amplitude increases from 10° to 20°, it can be seen that the starting vortex of the upper row moves upward nearing the plate edge. As a result, the lateral vortex spacing increases from 2.0 to $2.5H$ with an increase of the forcing amplitude. However, the increase of forcing amplitude at the same forcing frequency has no essential influence on the longitudinal vortex spacing, which is nearly the same at about $4.3H$. The variation of the longitudinal and lateral vortex spacing for the lock-on state with the forcing frequency and amplitude demonstrates the same trend as the experiments of Griffin and Ramberg (1976). The experiments of Griffin and Ramberg were conducted for flow across a circular cylinder oscillating transversely and horizontally.

The onset of vortex lock-on to the external forcing oscillation depends on the combination of the forcing frequency and amplitude. Fig. 12 shows the limits of lock-on regime bounded by the forcing frequency and angular displacement amplitude computed in the present study. In general, the forcing amplitude for the onset of lock-on increases with an

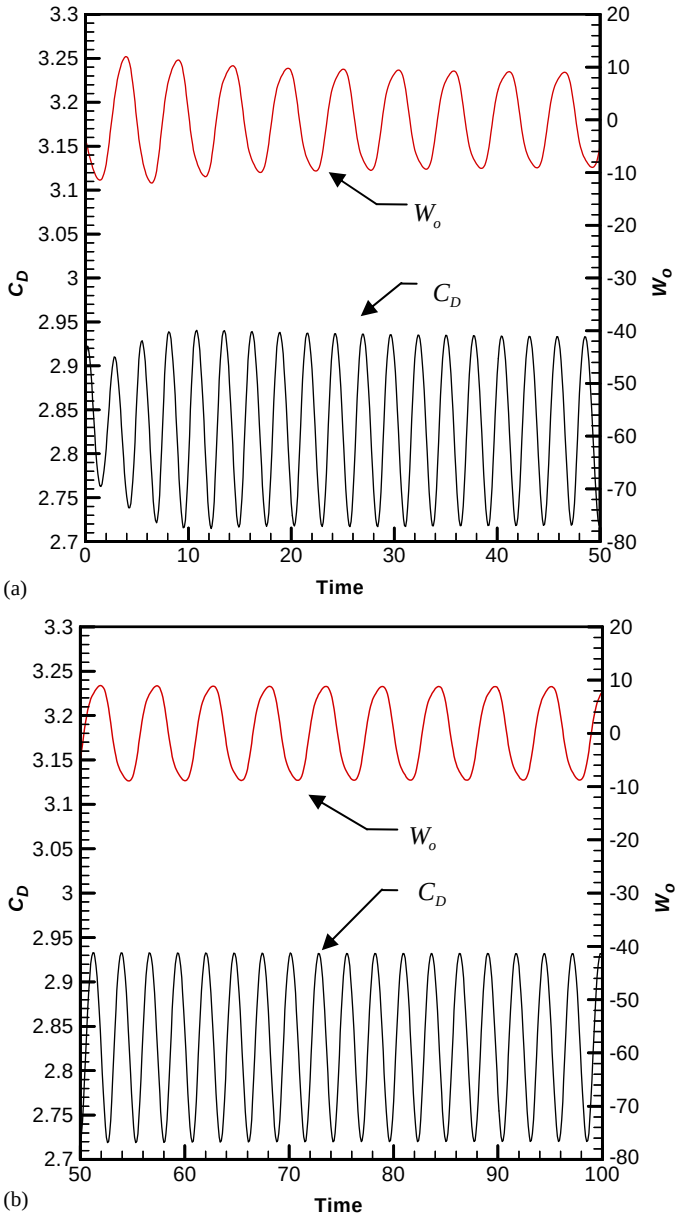

Fig. 7. Time histories of C_D and W_o leading to lock-on for $St_e/St_n = 1.040$ at $A_0 = 20°$: (a) dimensionless time 0–50; (b) dimensionless time 50–100.

increase in the difference between the forcing and natural shedding frequencies. But the approach from the upper forcing frequency requires smaller forcing amplitude than that from the lower frequency. The lock-on boundary, although computed at a lower Reynolds number $Re = 100$, appears to be in good agreement with the experiments of Chen and Fang (1998). The lock-on boundary obtained in the experiments were correlated from the selected data measured for $Re = 3600-9800$ at the same corrected free-stream velocity of 1.83 m/s for unbounded flow. Here, no attempt is made to interpret the above comparison as a result that the Reynolds number has little influence on the wake structure for the lock-on cases. This agreement, however, suggests that the Reynolds number effect on the lock-on boundary for the oscillating normal plate may not be as substantial as in the case of an oscillating circular cylinder in which the variability of the separation-point position adds a degree of freedom to complexity (Roshko, 1993). It is

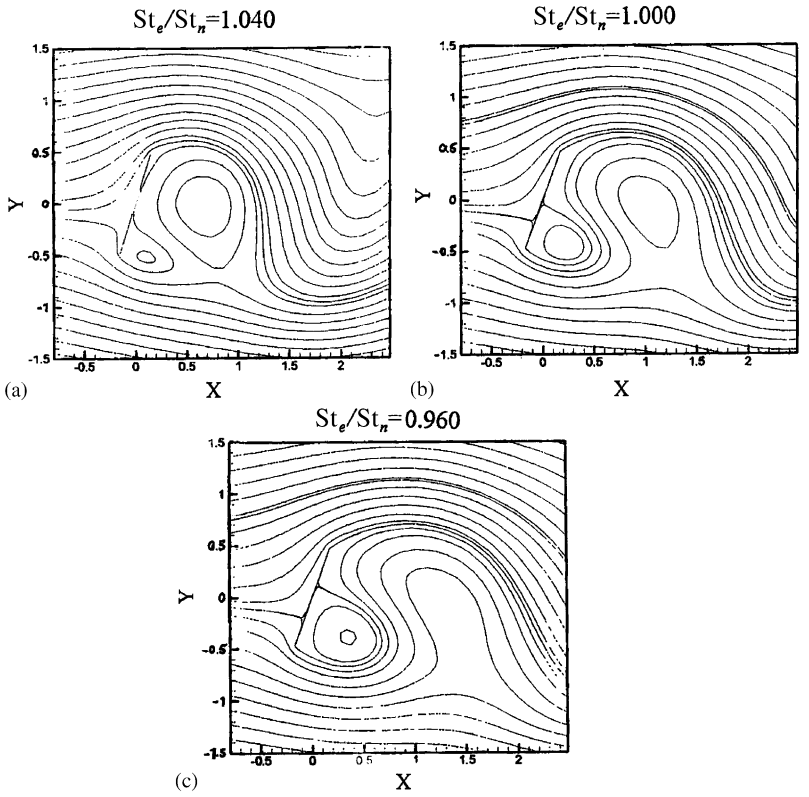

Fig. 8. (a)–(c) Streamline contours for $St_e/St_n = 1.040$, 1.0 and 0.960, respectively, at $A_0 = 20^\circ$.

conjectured that when the vortex shedding is locked-on to the oscillating normal plate at $St_e/St_n \approx 1$, the flow in the laboratory can be controlled to be more two-dimensional with organized vortex wake even at moderate Reynolds numbers and the lock-on boundary is mainly determined by the occurrence of strong resonance between the forcing oscillation and the organized large-scale vortices being shed, rather than the coalescence of secondary vortices (Cheng et al., 2001). Accordingly, the onset of lock-on may be less sensitive to the nonlinear transition in the separating shear layers than one may expect for the stationary case. Nevertheless, further numerical simulations and experiments covering higher Reynolds numbers and a wider range of forcing frequency are needed to attain a better understanding of the lock-on mechanism.

4. Conclusion

Numerical simulations have been carried out to investigate the lock-on of vortex shedding from a rotationally oscillating flat plate for two-dimensional laminar flow at $Re = 100$. The onset of vortex lock-on depends on the combination of the forcing frequency and amplitude of the oscillating plate. The time histories of drag coefficient as well as the surface vorticity at the rotation axis of the plate show amplitude modulation when the vortex shedding is non-locked-on to the motion of the plate oscillating at smaller forcing amplitude. Once the vortex shedding is in the lock-on regime, achieved by increasing the forcing amplitude, the modulation disappears and the time histories synchronize with the plate motion. It is found that the starting vortex tends to move toward the tip of the plate as the forcing amplitude increases, enlarging the lateral vortex spacing. On the other hand, the longitudinal vortex spacing shrinks as the forcing frequency increases. The limits of the lock-on regime bounded by the forcing frequency and angular displacement amplitude are found to agree well with the experiments of Chen and Fang (1998) conducted at higher Reynolds numbers ($Re = 3600-9800$), indicating the effect due to the Reynolds number in the range presented

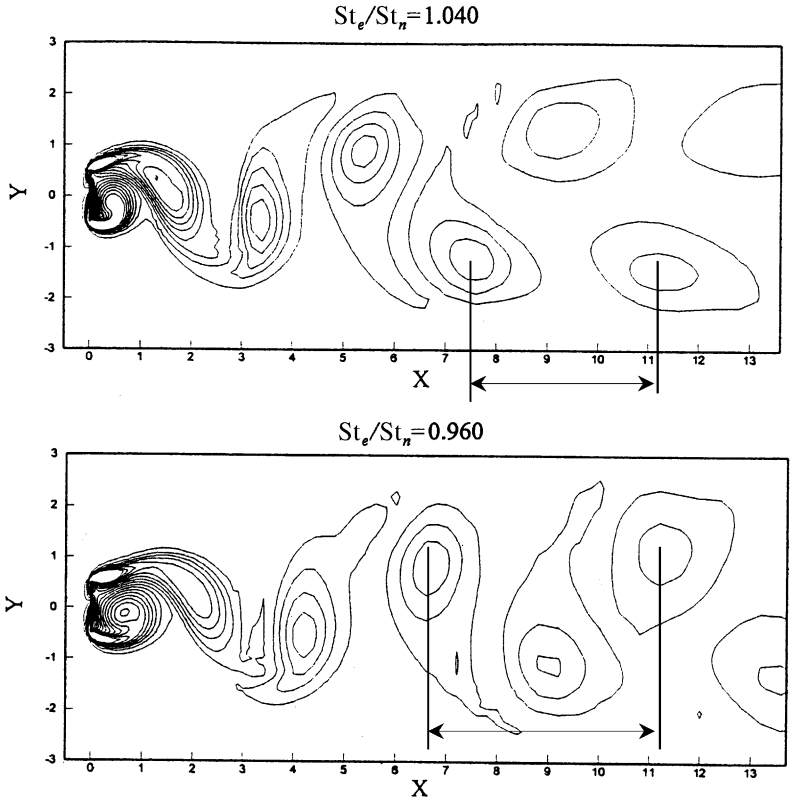

Fig. 9. Vorticity contours for $St_e/St_n = 1.040$ and 0.960 at $A_0 = 20^\circ$ and comparison of longitudinal vortex spacing.

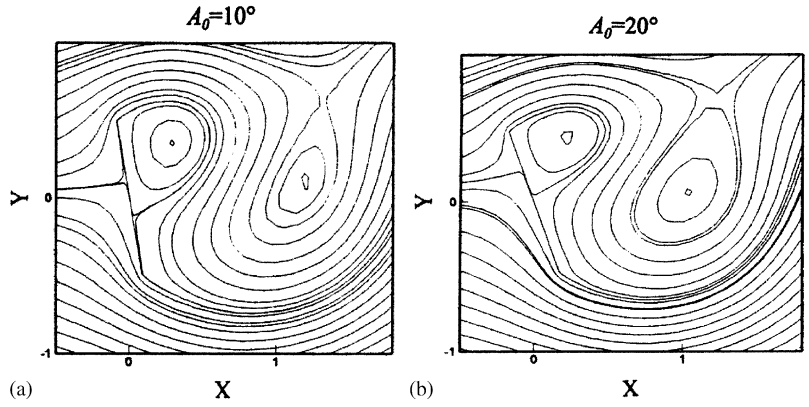

Fig. 10. Streamline contours for (a) $A_0 = 10^\circ$ and (b) 20° at $St_e/St_n = 1.0$.

may not be as substantial as in the case of an oscillating circular cylinder. Both the numerical and experimental studies show that the approach from the higher forcing frequency requires smaller forcing amplitude for lock-on than that from the lower frequency, and the numerical simulations show that the former results in larger amplitude of the drag and surface vorticity fluctuations.

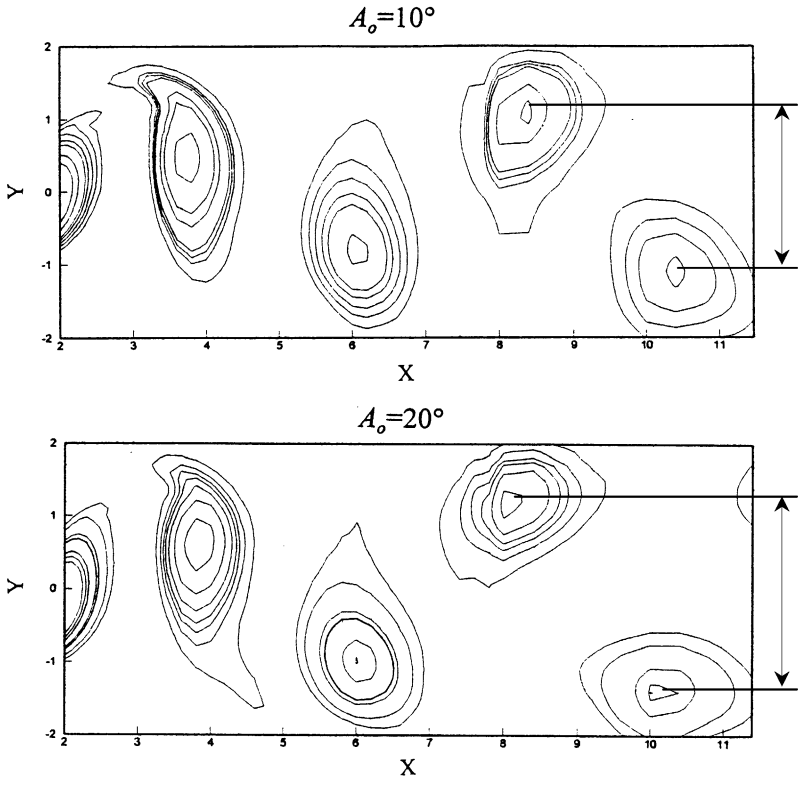

Fig. 11. Vorticity contours for $A_0 = 10$ and 20° at $St_e/St_n = 1.0$ and comparison of lateral vortex spacing.

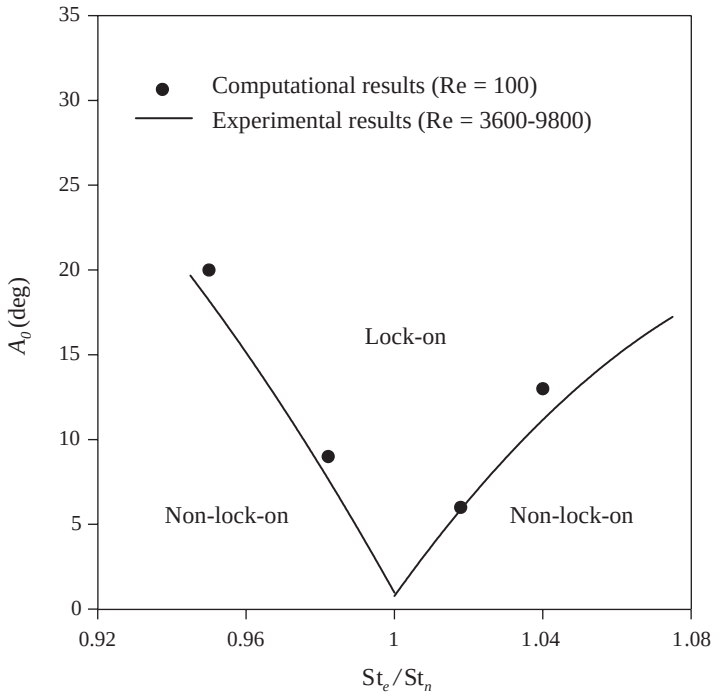

Fig. 12. Comparison of lock-on region determined by numerical study and experiments of Chen and Fang (1998).

Acknowledgments

The authors would like to thank the financial support for this study from the National Science Council of Taiwan under Contract Nos. NSC 89-2212-E005-027 and NSC 90-2212-E-005-025.

References

Anagnostopoulos, P., 2000. Numerical study of the flow past a cylinder excited transversely to the incident stream. Part 1: Lock-in zone, hydrodynamic forces and wake geometry. Journal of Fluids and Structures 14, 819–851.

Baek, S.-J., Sung, H.J., 2000. Quasi-periodicity in the wake of a rotationally oscillating cylinder. Journal of Fluid Mechanics 231, 275–300.

Blevins, R.D., 1990. Flow Induced Vibration, second ed. Van Nostrand Reinhold, New York.

Chen, J.M., Fang, Y.-C., 1998. Lock-on of vortex shedding due to rotational oscillations of a flat plate in a uniform stream. Journal of Fluids and Structures 15, 981–1007.

Cheng, M., Chew, Y.T., Luo, S.C., 2001. Numerical investigation of a rotationally oscillating cylinder in mean flow. Journal of Fluids and Structures 12, 779–798.

Choi, S., Choi, H., Kang, S., 2002. Characteristics of flow over a rotationally oscillating cylinder at low Reynolds number. Physics of Fluids 14, 2767–2777.

Chua, K., Lisoski, D., Leonard, A., Roshko, A., 1990. A numerical and experimental investigation of separated flow past an oscillating flat plate. In: Miller, J.A., Telionis, D.P. (Eds.), Proceedings of International Symposium in Nonsteady Fluid Dynamics, FED-vol. 92. ASME, New York, pp. 455–464.

Fang, Y.-C., Chen, J.M., 2000. Experimental study of vortex shedding and subharmonic lock-on for a rotationally oscillating flat plate. Journal of Wind Engineering and Industrial Aerodynamics 84, 163–180.

Filler, J.R., Marston, P.L., Mih, W.C., 1991. Response of the shear layers separating from a circular cylinder to small amplitude rotational oscillations. Journal of Fluid Mechanics 231, 481–499.

Griffin, O.M., Ramberg, S.E., 1976. Vortex shedding from a cylinder vibrating in line with an incident uniform flow. Journal of Fluid Mechanics 75, 257–271.

Karniadakis, G., Triantafyllou, G., 1989. Frequency selection and asymptotic states in laminar wakes. Journal of Fluid Mechanics 199, 441–469.

Mahfouz, F.M., Badr, H.M., 2000. Flow structure in the wale of a rotationally oscillating cylinder. ASME Journal of Fluids Engineering 122, 290–301.

Najjar, F.M., Balachandar, S., 1998. Low-frequency unsteadiness in the wake of a normal flat plate. Journal of Fluid Mechanics 370, 101–147.

Najjar, F.M., Vanka, S.P., 1995. Simulations of the unsteady separated flow past a normal flat plate. International Journal for Numerical Methods in Fluids 21, 525–547.

Ongoren, A., Rockwell, D., 1988a. Flow structure from an oscillating cylinder. Part 1: Mechanisms of phase shift and recovery in the near wake. Journal of Fluid Mechanics 191, 197–223.

Ongoren, A., Rockwell, D., 1988b. Flow structure from an oscillating cylinder. Part 2: Mode competition in the near wake. Journal of Fluid Mechanics 191, 225–245.

Panton, R.L., 1984. Incompressible Flow. Wiley, New York.

Roshko, A., 1993. Perspectives on bluff body aerodynamics. Journal of Wind Engineering and Industrial Aerodynamic 49, 79–100.

Tamaddon-Jahromi, H.R., Townsned, P., Webster, M.F., 1994. Unsteady viscous flow past a flat plate orthogonal to the flow. Computers & Fluids 23, 433–446.

Taneda, S., Honji, T., 1971. Unsteady flow past a flat plate normal to the direction of motion. Journal of the Physical Society of Japan 34, 262–272.

Tokumaru, P.T., Dimotakis, P.E., 1991. Rotary oscillation control of a cylinder wake. Journal of Fluid Mechanics 224, 77–90.